Journal of Zhejiang University SCIENCE A
ISSN 1673-565X (Print); ISSN 1862-1775 (Online)
www.zju.edu.cn/jzus; www.springerlink.com
E-mail: jzus@zju.edu.cn

Multi-physics coupling field finite element analysis on giant magnetostrictive materials smart component*

Zhang-rong ZHAO[†1,2], Yi-jie WU[†‡1], Xin-jian GU[1], Lei ZHANG[1], Ji-feng YANG[1]

([1]*State Key Laboratory of Fluid Power Transmission and Control, Modern Manufacture Engineering Institute, Zhejiang University, Hangzhou 310027, China*)

([2]*Department of Mechanical & Electronic, North China Institute of Science and Technology, Beijing 101601, China*)

[†]E-mail: zhaozhangrong@sina.com; wyj1116@zju.edu.cn

Received June 26, 2008; Revision accepted Sept. 27, 2008; Crosschecked Feb. 26, 2009

Abstract: This study presents a new method to solve the difficult problem of precise machining a non-cylinder pinhole of a piston using embedded giant magnetostrictive material (GMM) in the component. We propose the finite element model of GMM smart component in electric, magnetic, and mechanical fields by step computation to optimize the design of GMM smart component. The proposed model is implemented by using COMSOL multi-physics V3.2a. The effects of the smart component on the deformation and the system resonance frequencies are studied. The results calculated by the model are in excellent agreement (relative errors are below 10%) with the experimental values.

Key words: Smart component, Giant magnetostrictive, Finite element method (FEM) modeling, Non-cylinder piston pinhole, Multi-physics coupling field

doi:10.1631/jzus.A0820492 **Document code:** A **CLC number:** O343.2; TM15

INTRODUCTION

The most important part of an engine, the piston directly influences the engine's performance and even the whole performance of the power transmission system. When the fuel consumption, output power and rotating speed of the engine increase, the piston bears increasing gas pressure and inertia force, which makes the piston pinhole bear an increasing load. To improve the bearing capacity of the piston pinhole, the shape of the hole can be gradually developed towards a pipe socket, ellipse and component hole (Suhara *et al.*, 1996; Silva, 2006). This non-columniform pinhole is called as a "non-cylinder pinhole". At present, the mature methods of machining the non-cylinder pinhole include lever tool bar machining, eccentric tool bar machining, eccentric spindle machining, and profiling or boring machining (Weng and Weng, 1998; Hu *et al.*, 1999). All these technologies use mechanical components and profiling, leading to some disadvantages, such as complicated structures, high-standard demands of manufacturing accuracy for parts, abrasion with long operation time, uncertain manufacturing accuracy. According to Hu *et al.*(1999), Zhang *et al.*(2003) and Zhai *et al.*(2007), piezoceramics, giant magnetostrictive materials (GMM) and deformation of the structure can be used to machine a non-cylinder pinhole. This, however, leads to a very complicated structure. In this study, a smart component for precise machining a non-cylinder hole is designed by embedding GMM directly into the component.

Since there are multi-physics coupling fields, such as electric, magnetic, and mechanical fields in the GMM, the key point to optimize the design of the GMM component is the computation of the

‡ Corresponding author

* Project supported by the National Natural Science Foundation of China (No. 50575205), the Hi-Tech Research and Development (863) Program of China (Nos. 2006AA04Z233 and 2007AA04Z101), the Doctoral Foundation of Ministry of Education of China (No. 20070335204), and the Zhejiang Provincial Natural Science Foundation of China (No. Z1080537)

multi-physics coupling fields. Current commercial softwares, such as ANSYS, NASTRAN, SAP, and COMSOL multi-physics only include the coupling computations of the piezoceramics electric and mechanical fields, but do not have the coupling computations of the electric, magnetic and mechanical fields needed to simulate the GMM. ATILA is a professional software aimed particularly for piezoceramics and giant magnetostrictive transducer design and can be used to calculate the coupling computations of the electric, magnetic and mechanical fields and fluid linearity (Claeyssen *et al.*, 1997; Heinonen *et al.*, 2005). It separates the GMM magnetic field into the source magnetic field produced by driven coil and the magnetic field produced by magnetization. The source magnetic field is depicted by the predefined current function. However, the function is not able to depict magnetic distribution in all situations (Claeyssen *et al.*, 1990). It can only be used for transducers, not for the other GMM actuators.

Many researchers have done a lot of work with the finite element analysis (FEA) of the GMM multi-physics coupling field and proposed some valuable models (Kaltenbacher *et al.*, 2001; Besbes *et al.*, 2001; Karim *et al.*, 2004; Ghosh and Gopalakrishnan, 2007; Galopin *et al.*, 2008). Dean *et al.*(2006) and Watts *et al.*(1997) stated that magnetostrictive and thermal components of the mechanical strains of the GMM can be separated as internal components of strain in order to properly implement the FEA of the GMM beam. However, constant magnetostrictive strain components cannot truly show the distribution of the magnetostrictive strain in the GMM. Mo *et al.*(2000) simulated the GMM as piezoceramics in order to implement FEA of the giant magnetostrictive transducer using ANSYS. Because the magnetic field that drives the GMM is produced by the drive coil current and the input variable is current, an approximate error is going to be generated during computation. Benatar and Flatau (2005) and Perez-Aparicio and Sosa (2004) used a magnetic vector potential to compute the coupling of the electric, magnetic and mechanical fields in the GMM. Regardless, the number of degrees of freedom (DOFs) on a node can be excessive, and too much memory is occupied for the 3D structural computation. As a result, calculation speeds are slow and the memory often runs out. Under these circumstances, the coupling of the three above-mentioned fields in the GMM is decomposed by first computing the magnetic field created by the drive coil, and then by computing the magnetic and mechanical coupling fields, which is described in this study. The coupling field computation of the magnetic field consists of the source and demagnetizing fields created by the drive coil current and demagnetizing, respectively. The demagnetizing field is described by using a reduced magnetic potential. The above computing is implemented by using a finite element weak form formulation with COMSOL multi-physics V3.2a. For the designed smart component, its static deformation, natural frequencies and modes of vibration are studied using 3D finite element models as presented in this study. The presented finite element models are verified by comparing the FEM calculations and experimental results.

MACHINING PRINCIPLE OF THE SMART COMPONENT FOR A NON-CYLINDER PINHOLE

We present a new structure for machining a non-cylinder pinhole by embedding the GMM directly into the component. The schematic diagram of the smart component after distortion is shown in Fig.1.

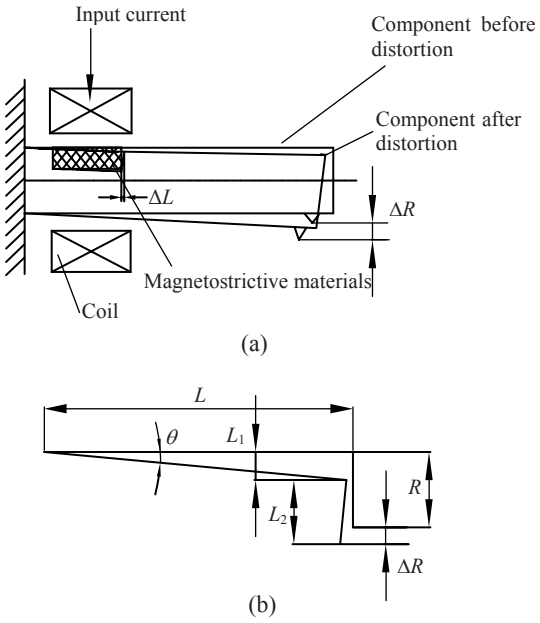

Fig.1 (a) Schematic diagram of the embedded GMM smart component after distortion; (b) A tiny turning angle θ of the smart component

Under the driving current, the GMM elongates and bends the smart component generating a radial feed. By controlling the input current, the precise machining of the non-cylinder pinhole can be achieved. The magnetostrictive constant $\boldsymbol{\lambda}$ of the GMM is the function of the driven magnetic field $\boldsymbol{H}$, i.e., $\boldsymbol{\lambda}=F(\boldsymbol{H})$. The drive coil current and the magnetic field has the approximate functional relation $\boldsymbol{H}=n\boldsymbol{I}$, therefore, the magnetostrictive constant $\boldsymbol{\lambda}$ is the function of the drive coil current, i.e., $\boldsymbol{\lambda}=F(n\boldsymbol{I})$. A small turning angle θ is produced by the smart component bending. Fig.1 shows that:

$$L_1 = L\sin\theta,$$
$$L_2 = R\cos\theta,$$
$$\Delta R = L_1 + L_2 - R = L\sin\theta + R\cos\theta - R.$$

Because θ is small, it can be concluded that $\sin\theta=\theta$, $\cos\theta=1$ and $\Delta R=L\theta$. Moreover, θ is proportional to ΔL, i.e., $\theta=k\Delta L$, where k is the scale factor. Therefore, the radial increment can be obtained by $\Delta R=kL\Delta L$. Since $\lambda=\Delta L/L'$, where L' is the length of the GMM, the radial increment is the function of the current, i.e., $\Delta R=kLL'F(n\boldsymbol{I})$. As can be seen from the above equations, the desired radial feed to machine the non-cylinder pinhole can be achieved by controlling the drive coil current.

FINITE ELEMENT MODEL OF THE GMM SMART COMPONENT

To accurately analyze the performance of the smart component driven by embedding the GMM, the coupling effects of the electric, magnetic, and mechanical fields in the GMM should be taken into consideration. In order to reduce the DOFs needed to resolve the problem, the three fields coupling effects are computed in two steps. Firstly, the magnetic field driven by the coil current is computed, where the node variables are the magnetic vector potentials (A_x, A_y, A_z). Secondly, the mechanical and magnetic coupling fields are solved, where the node variables are displacements (u, v, w) and reduced magnetic potential (ϕ).

Maxwell's equations are a set of equations stating the relationship between the fundamental electromagnetic quantities. The magnetic field produced by the coil satisfies Maxwell's equations:

$$\nabla\times\boldsymbol{H}=\boldsymbol{J}, \tag{1}$$
$$\nabla\boldsymbol{B}=0, \tag{2}$$

where $\boldsymbol{H}$, $\boldsymbol{J}$ and $\boldsymbol{B}$ are the magnetic field intensity, source current density and magnetic flux density, respectively. The relationship between the magnetic field intensity and magnetic flux density is as follows:

$$\boldsymbol{B}=\boldsymbol{\mu}\boldsymbol{H}, \tag{3}$$

where $\boldsymbol{\mu}$ is permeability of the medium. Below is the finite element equation in weak form:

$$\int_V(\delta\boldsymbol{A}^{\mathrm{T}}\boldsymbol{J}-\delta\boldsymbol{B}^{\mathrm{T}}\boldsymbol{H})\mathrm{d}V+\int_S\delta\boldsymbol{A}^{\mathrm{T}}\boldsymbol{H}_{\mathrm{s}}\mathrm{d}S=0. \tag{4}$$

The magnetic field $\boldsymbol{H}$ in the GMM consists of the source magnetic field $\boldsymbol{H}_{\mathrm{s}}$ produced by the coil and the magnetic field H_{M} produced by demagnetizing, i.e.,

$$\boldsymbol{H}=\boldsymbol{H}_{\mathrm{s}}+\boldsymbol{H}_{\mathrm{M}}, \tag{5}$$

where $\boldsymbol{H}_{\mathrm{M}}=-\nabla\phi$, ϕ is reduced magnetic potential. Therefore, the magnetic field of the GMM can be expressed as:

$$\boldsymbol{H}=-\nabla\phi+\boldsymbol{H}_{\mathrm{s}}. \tag{6}$$

In the most general way, the behavior of GMM is nonlinear. However, the behavior of most giant magnetostrictive devices may be rather well described using a linear theory, because the active materials are biased. The bias conditions are defined by the magnetic bias and the mechanical pre-stress, applied along the GMM rod axis. Considering only the variations around this initial bias state, coupling relations between the mechanical and the magnetic fields of the GMM can be expressed by linear constitutive equations:

$$\boldsymbol{T}=\boldsymbol{C}^{\mathrm{H}}\boldsymbol{S}-\boldsymbol{e}\boldsymbol{H}, \tag{7}$$
$$\boldsymbol{B}=\boldsymbol{e}^{\mathrm{T}}\boldsymbol{S}+\boldsymbol{\mu}^{\mathrm{s}}\boldsymbol{H}, \tag{8}$$

where $\boldsymbol{T}$, $\boldsymbol{S}$, $\boldsymbol{H}$, $\boldsymbol{B}$, $\boldsymbol{C}^{\mathrm{H}}$, $\boldsymbol{e}$, $\boldsymbol{\mu}^{\mathrm{s}}$ are stress tensor, strain tensor, magnetic field intensity, magnetic flux density,

elasticity modulus under constant magnetic field, piezomagnetic constants, and permeability under constant strain, respectively. Based on the Hamilton's principle, the dynamical equations of the GMM can be derived:

$$\int_{t_1}^{t_2} \delta L \mathrm{d}t = 0, \tag{9}$$

where δ, t_1 and t_2 are the first order differential operator, start time and end time, respectively. The Lagrangian term L is determined by the energies available in the GMM:

$$L = E_{\mathrm{kin}} - E_{\mathrm{s}} + W, \tag{10}$$

where the kinetic energy E_{kin}, potential energy E_{s} and energy W generated by an external force can be expressed as:

$$E_{\mathrm{kin}} = \frac{1}{2}\int \rho \dot{\boldsymbol{u}}^2 \mathrm{d}V, \tag{11}$$

$$E_{\mathrm{s}} = \frac{1}{2}\int (\boldsymbol{S}^{\mathrm{T}}\boldsymbol{T} - \boldsymbol{H}^{\mathrm{T}}\boldsymbol{B})\mathrm{d}V, \tag{12}$$

$$W = \int_V \boldsymbol{u}^{\mathrm{T}} \boldsymbol{f}_{\mathrm{b}} \mathrm{d}V + \int_{S_1} \boldsymbol{u}^{\mathrm{T}} \boldsymbol{f}_{\mathrm{s}} \mathrm{d}S_1 - \int_{S_2} \phi \boldsymbol{B}_{\mathrm{s}} \mathrm{d}S_2, \tag{13}$$

where ρ, $\dot{\boldsymbol{u}}$, $\boldsymbol{S}$, $\boldsymbol{T}$, $\boldsymbol{H}$, $\boldsymbol{B}$, $\boldsymbol{f}_{\mathrm{b}}$, $\boldsymbol{f}_{\mathrm{s}}$, $\boldsymbol{B}_{\mathrm{s}}$, and ϕ are mass density, velocity vector, strain tensor, stress tensor, magnetic field intensity, magnetic flux density, vector of the mechanical body force, the prescribed vector of the mechanical surface forces on the surface S_1, the prescribed magnetic flux density on the surface S_2 and the reduced magnetic potential, respectively. By substituting Eqs.(6)~(8) and Eqs.(10)~(13) into Eq.(9), we can obtain:

$$\begin{aligned}\int_V [&\delta \boldsymbol{S}^{\mathrm{T}} \boldsymbol{C}^H \boldsymbol{S} - \delta \boldsymbol{S}^{\mathrm{T}} \boldsymbol{e} \boldsymbol{H} - \delta(-\nabla\phi + \boldsymbol{H}_{\mathrm{s}})^{\mathrm{T}} \boldsymbol{e}^{\mathrm{T}} \boldsymbol{S} \\ &- \delta(-\nabla\phi + \boldsymbol{H}_{\mathrm{s}})^{\mathrm{T}} \boldsymbol{\mu}^{\mathrm{s}} (-\nabla\phi + \boldsymbol{H}_{\mathrm{s}}) + \rho \delta \boldsymbol{u}^{\mathrm{T}} \ddot{\boldsymbol{u}} \\ &- \delta \boldsymbol{u}^{\mathrm{T}} \boldsymbol{f}_{\mathrm{b}}]\mathrm{d}V - \int_{S_1} \delta \boldsymbol{u}^{\mathrm{T}} \boldsymbol{f}_{\mathrm{s}} \mathrm{d}S_1 + \int_{S_2} \delta \phi \boldsymbol{B}_{\mathrm{s}} \mathrm{d}S_2 = 0.\end{aligned} \tag{14}$$

Eq.(14) is the finite element equation in the weak form for the coupling magnetic and mechanical fields of the GMM.

COMSOL multi-physics V3.2a is a professional finite element numerical analysis package. Different modules can be selected freely and simultaneously to simulate coupling analysis of any combined physical fields. To get the static deformations, natural frequencies and modes of vibration of the smart component, three different modules were used. One module was structural mechanics; the other two modules were weak form application modes to realize the Eqs.(4) and (14), respectively. Variables in Eq.(4) were $\{A_x, A_y, A_z\}$ and those in Eq.(14) were $\{u, v, w, \phi\}$.

SIMULATION AND EXPERIMENTAL VERIFICATION

A radial bending of over 60 μm and resonance frequency over 100 Hz, under 5-A input current and 80-N resisting force of the tool are required to be realized by the smart component. Fig.2 shows the structure of the smart component. It consists of a component made of 45# steel with radiuses of 15 and 310 mm in length, a semi-cylinder GMM rod with radiuses of 15 and 60 mm in length, a coil with 39 mm inner and 73 mm outer radiuses, and 1365 turns.

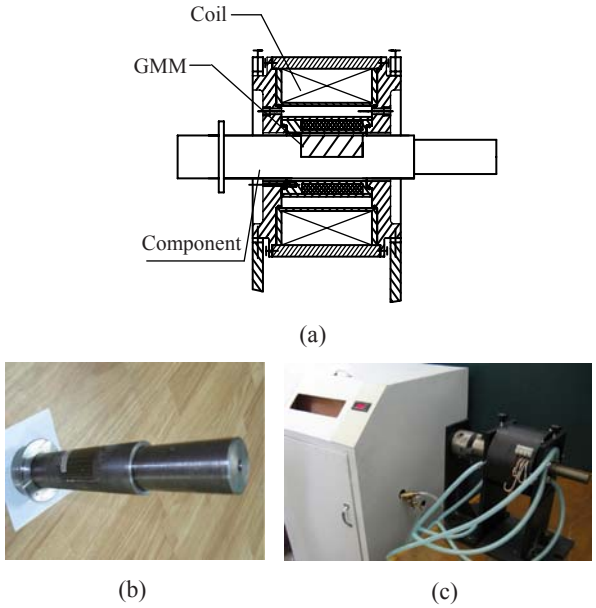

Fig.2 (a) Scheme of the smart component system; (b) GMM smart component; (c) Experiment table

The smart component has a nonaxisymmetrical structure because of the existence of the semi-cylindrical GMM, as shown in Fig.2a. Therefore, the

structure is analyzed by using a 3D model. The material properties used in the finite element model are listed in Tables 1 and 2. These coefficients of Terfenol-D are obtained at about 60 kA/m magnetic bias and 0 Pa mechanical prepress. The 3D mesh of the structure and the distribution of the magnetic field are shown in Figs.3 and 4, respectively.

Table 1 Material properties of 45# steel of the smart component

Parameter	Value
Density (kg/m^3)	7800
Young's modulus (GPa)	200
Poisson's ratio	0.3
Relative permeability	1000

Table 2 Material properties of GMM (Terfenol-D)

Parameter	Value	Parameter	Value
Density	9200	c_{11}	3.361
μ_{11}	35.17	c_{12}	2.340
μ_{33}	25	c_{13}	2.566
d_{31}^*	−2.557	c_{33}	3.067
d_{33}^*	5.090	c_{44}	1.894
d_{15}^*	1.145	c_{66}	0.510

μ_{11} and μ_{33}: permeability constants ($\times10^{-7}$ H/m); d_{31}^*, d_{33}^*, and d_{15}^*: piezomagnetic constants ($\times10^{-9}$ m/A); c_{11}, c_{12}, c_{13}, c_{33}, c_{44}, and c_{66}: elasticity constants ($\times10^{12}$ Pa)

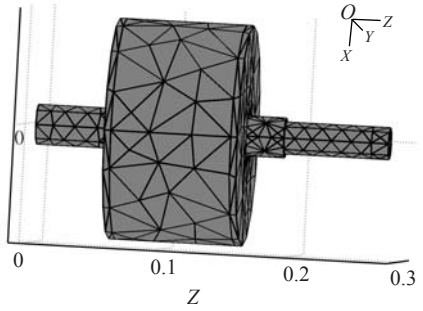

Fig.3 3D mesh of the smart component

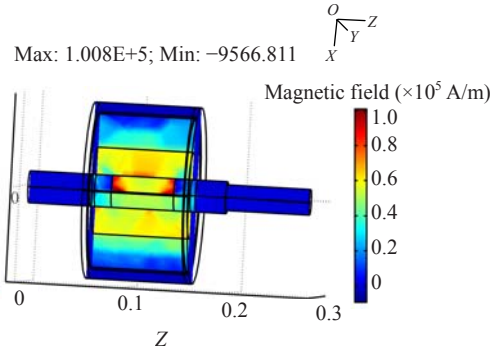

Fig.4 *Z* axis distribution of the magnetic field intensity of the smart component. Slice: magnetic field, *z* component

According to the relationship between magnetic field and magnetostrictive strain of Terfenol-D that is adopted by GMM, an approximate linear area is chosen during design. The driven magnetic field is 20~80 kA/m. As shown in Fig.4, the axial magnetic field intensity is around 60 kA/m. Therefore, the designed GMM smart component meets the requirement of GMM linear working area. Figs.5a and 5b show the *x*-direction bending of the smart component without any resisting force and under an 80-N resisting force of the tool, respectively. The line plot of the *X* axis deformation along the central axis of the smart component is shown in Fig.6.

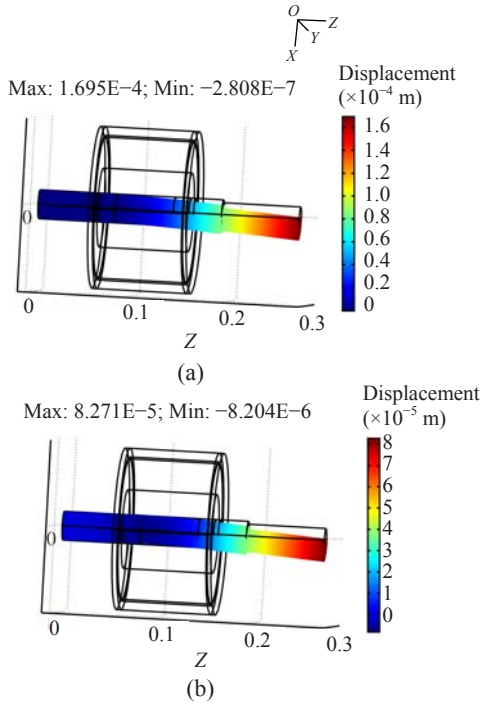

Fig.5 *X* axis deformation of the smart component (a) without any resisting force of the tool and (b) under an 80-N resisting force of the tool. Boundary: *x*-displacement (m); deformation: displacement

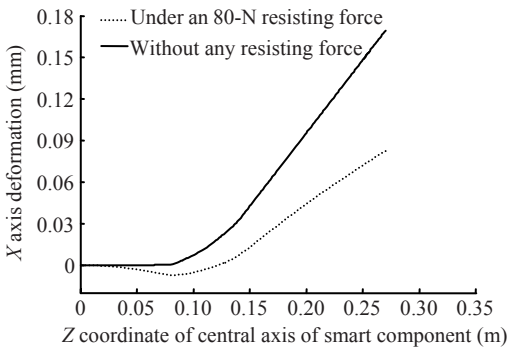

Fig.6 *X* axis deformation along the central axis of smart component

As shown in Figs.5 and 6, the maximum bending deformation is 169 μm without any resisting force of the tool, and 82 μm under an 80-N resisting force of the tool. The GMM smart component designed in this study is mainly used to machine a non-cylinder pinhole of a piston. According to current sizes of non-cylinder pinholes, machining non-cylinder pinholes only needs a tool having 50 μm of radial feed. Therefore, 82 μm radial bending deformation can implement the machining of a non-cylinder pinhole. This meets the design requirement so that a piston pinhole with sufficient dimension can be created. Three experiments were done under different currents to test the bending deformation of the smart component. The comparison of the simulation results between the average values of the three experiment results are shown in Fig.7.

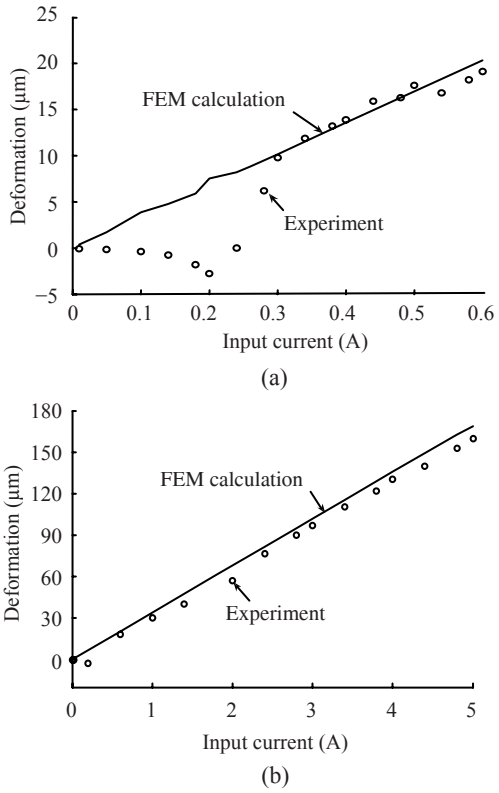

Fig.7 Simulation and experimental results as a function of input current. (a) 0~0.6 A; (b) 0~5 A

As shown in Fig.7a, when the input current is between 0~0.3 A, the starting radius increment shifts in the negative direction with the increasing of the current. When the current approaches 0.24A, the radius increment returns to 0, and then shifts in a positive direction. Also, between 0~0.3 A, the simulated deformation changes from 0 to 10 μm, different from the experimental result, which relates to the internal mechanism of the GMM and needs further study. During this period, the test result shows the GMM smart component having strong nonlinear relationship. However, the computation result shows linear relationship due to the finite element model using linear constitutive relation. The maximum errors between those differences reach 10 μm. Therefore, using the linear finite element model in this period cannot reflect the performance of the GMM smart component. In addition, considering nonlinearity will make the design for the control system much more complex. In a practical application, this range should be abandoned. When the current is between 0.3~5.0 A, the results calculated by the model are in excellent agreement (relative errors are below 10%) with the experimental values, as shown in Fig.7b. As shown in Fig.7, input current and output deformation of the GMM smart component have a nonlinear relation during input current of 0~5 A. However, during an input current of 0.3~5.0 A, it has good linear relation with output deformation. Therefore, although the GMM smart component has nonlinear feature, it shows approximate linear relation during a certain period.

The first six resonance frequencies of the system were calculated using modal analysis and were 308.99, 321.65, 1550.21, 1626.36, 3057.48, and 3905.53 Hz, respectively. The corresponding modes of vibration are shown in Fig.8.

As shown in Fig.8, the minimum resonance frequency of the smart component is 309 Hz. The maximum rotating speed of the smart component in the boring machine is 3000 r/min, which corresponds to the frequency response of the smart component under 50 Hz shown in Fig.9. Fig.10 shows the maximum deformation of the GMM smart component as a function of frequency. Fig.9 shows that the maximum deformation is 172.5 μm at 50 Hz. Fig.10 shows that resonance will occur at 309, 321, 1550, 1626, 3057, and 3906 Hz when the input signal frequency of GMM smart component is 0~5000 Hz. Resonance does not occur when the frequency is less than 300 Hz. Therefore, the dynamic performance of the component satisfies the requirement of machining.

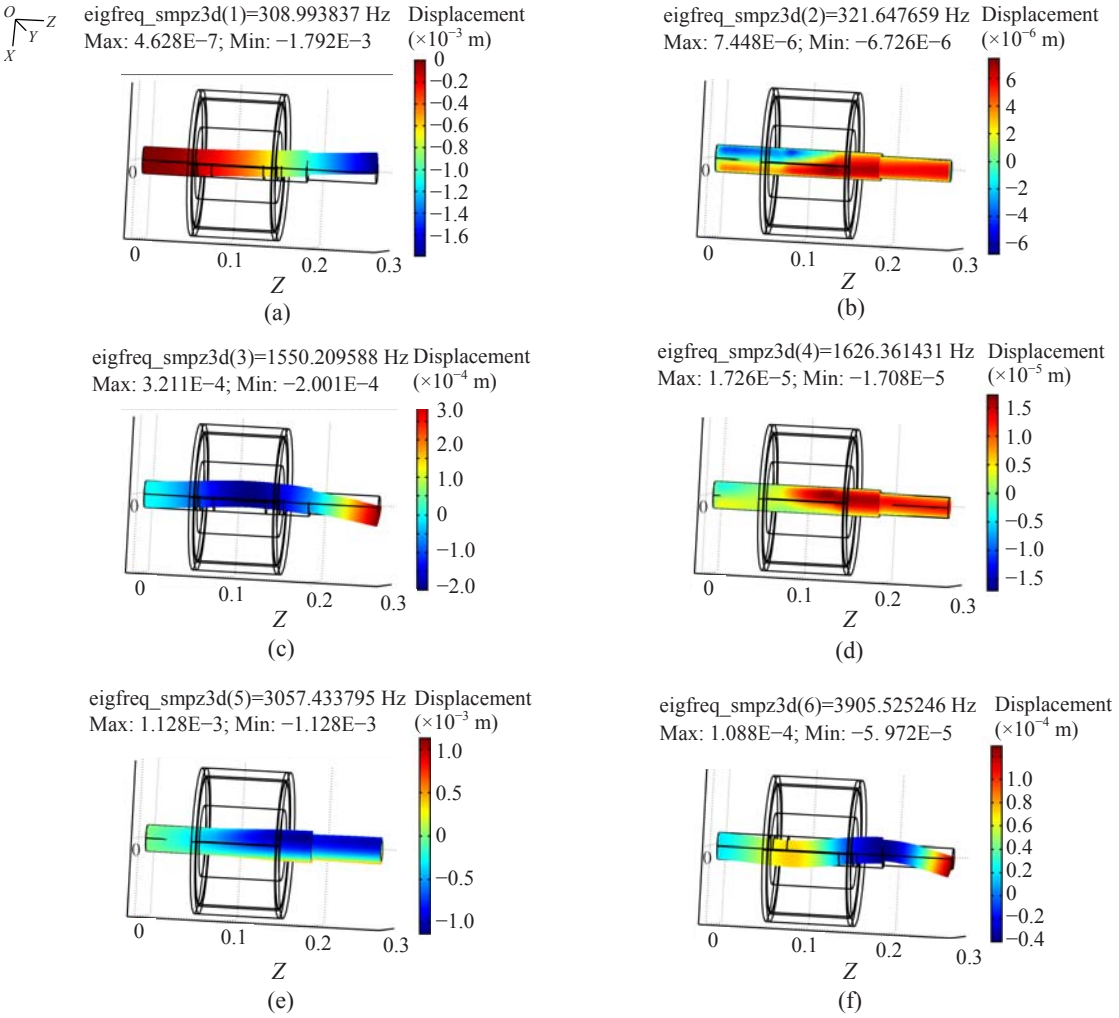

Fig.8 (a)~(f) First six resonance frequencies and modes of vibration of the smart component, respectively. Boundary: *x*-displacement (m); deformation: displacement

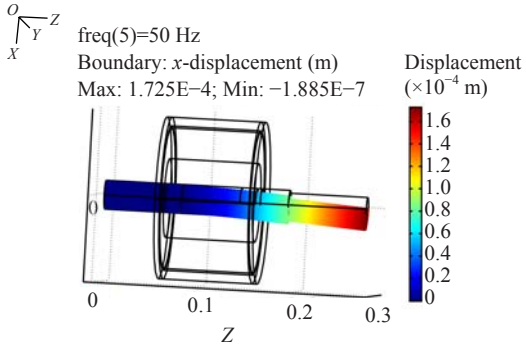

Fig.9 Deformation of the smart component under 50 Hz

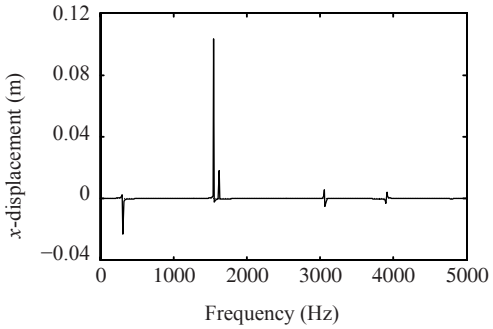

Fig.10 Frequency response of the GMM smart component as a function of frequency

CONCLUTION

A smart component for precise machining a non-cylinder pinhole is presented and the machining theory is analyzed. In order to reduce the DOFs needed to simulate the nodes, a step method was introduced. First, the magnetic field produced by the coil was computed. Second, the coupling of the

magnetic and the mechanical fields of the GMM were computed to establish the finite element model of the whole GMM electric, magnetic, and mechanic fields. COMSOL multi-physics V3.2a finite element software with weak form equation computations was used. The designed smart component reaches the required goal according to the static and modal analysis. The experimental results show the validness of the finite element modeling proposed here. The model is in good correspondence (relative errors are below 10%) for the applied design of the GMM. The model presented in this study can be implemented to aid the design of the GMM smart component, and can be applied for the GMM actuator design in other application fields. For example, it can be used to design GMM sonar transducer and GMM electromagnetic valve. Our research group implemented the design for the GMM smart component using this model, and the system control part for machining a non-cylinder pinhole of a piston is in further study. In this study, only the coupling of the electric, magnetic, and mechanical fields is implemented in the model. It is necessary to further study the coupling of the electric, magnetic, mechanical, and thermal fields. In addition, the model is using a linear constitutive relation, which can be used by assuming that the smart component is working in a certain linear area. If the whole area of the GMM would to be described, further investigation is needed to establish a nonlinear finite element model.

References

Benatar, J.G., Flatau, A.B., 2005. FEM implementation of a magnetostrictive transducer. *Smart Structures and Materials*, *Proc. of SPIE*, **5764**:482-493. [doi:10.1117/12.600003]

Besbes, M., Ren, Z., Razek, A., 2001. A generalized finite element model of magnetostriction phenomena. *IEEE Transactions on Magnetics*, **37**(5):3324-3328. [doi:10.1109/20.952605]

Claeyssen, F., Bossut, R., Boucher, D., 1990. Modeling and Characterization of the Magnetostricitive Coupling. Pro. Int. Work. Power Transducers for Sonics and Ultrasonics, Toulon, France, p.132-151.

Claeyssen, F., Lhermet, N., le Letty, R., Bouchilloux, P., 1997. Actuators, transducers and motors based on giant magnetostrictive materials. *Journal of Alloys and Compounds*, **258**:61-73. [doi:10.1016/S0925-8388(97)00070-4]

Dean, J., Gibbs, M.R.J., Schrefl, T., 2006. Finite-element analysis on cantilever beams coated with magnetostrictive material. *IEEE Transactions on Magnetics*, **42**(2):283-288. [doi:10.1109/TMAG.2005.861322]

Galopin, N., Mininger, X., Bouillault, F., Daniel, L., 2008. Finite element modeling of magnetoelectric sensors. *IEEE Transactions on Magnetics*, **44**(6):834-837. [doi:10.1109/TMAG.2008.915781]

Ghosh, D.P., Gopalakrishnan, S., 2007. A superconvergent finite element for composite beams with embedded magnetostrictive patches. *Composite Structures*, **79**(3):315-330. [doi:10.1016/j.compstruct.2006.01.007]

Heinonen, E., Juuti, J., Leppävuori, S., 2005. Characterization and modelling of 3D piezoelectric ceramic structures with ATILA software. *Journal of the European Ceramic Society*, **25**:2467-2470. [doi:10.1016/j.jeurceramsoc.2005.03.083]

Hu, D.J., Liu, R.M., Li, X.Q., Xu, L.M., 1999. Research and development of full automatic CNC special machine for boring piston pin hole. *Modular Machine Tool and Automatic Manufacturing Technique*, **1**:27-30 (in Chinese).

Kaltenbacher, M., Schneider, S., Simkovics, R., 2001. Nonlinear Finite Element Anlysis of Magnetostrictive Transducers. Proceedings of SPIE's 8th Annual International Symposium on Smart Structures and Materials, Newport Beach, CA, USA, **4326**:160-168. [doi:10.1117/12.436469]

Karim, A., Mondher, B., Frederic, B., 2004. 3D FEM of magnetostriction phenomena using coupled constitutive laws. *International Journal of Applied Electromagnetics and Mechanics*, **19**:367-371.

Mo, X.P., Zhu, H.Q., Liu, J.G., 2000. Terfenol-D giant magnetostrictive transducer simulation by finite element method. *Applied Acoustics*, **19**(4):5-8 (in Chinese).

Perez-Aparicio, J.L., Sosa, H., 2004. A continuum three dimensional, fully coupled, dynamic, non-linear finite element formulation for magnetostrictive materials. *Smart Materials and Structures*, **13**(3):493-502. [doi:10.1088/0964-1726/13/3/007]

Silva, F.S., 2006. Fatigue on engine pistons—A compendium of case studies. *Engineering Failure Analysis*, **13**:480-492. [doi:10.1016/j.engfailanal.2004.12.023]

Suhara, T., Takei, T., Takiguti, M., 1996. Characteristics of friction force on piston pin boss bearings. *JSAE Review*, **17**(4):453. [doi:10.1016/S0389-4304(96)80677-1]

Watts, R., Gibbs, M.R.J., Karl, W.J., 1997. Finite-element modeling of magnetostrictive bending of a coated cantilever. *Applied Physics Letters*, **70**(19):2607-2609. [doi:10.1063/1.118932]

Weng, J.Y., Weng, S.Y., 1998. Machining principle and equipment of non-cylinder pin hole of piston. *Shanghai Machine Tool*, **1**:22-24 (in Chinese).

Zhai, P., Zhang, X.R., Wang, H.T., Qin, L., Wang, X.L., 2007. Research on machining principle for non-cylinder piston pin hole based on GMM. *Piezoelectric & Acoustooptics*, **29**(1):125-128 (in Chinese).

Zhang, K., Hu, D.J., Ma, H.Q., 2003. Research on boring mechanism for piston noncircular pin hole. *Modular Machine Tool and Automatic Manufacturing Technique*, **8**:4-8 (in Chinese).